WORLD CONFERENCE ON TIMBER ENGINEERING 2025
BRISBANE, AUSTRALIA
Advancing Timber for the Future Built Environment

STEEL BAR-TIMBER COMPOSITE BEAM-COLUMN CONNECTION ADOPTING STEEL DAMPER

Masanori Nakamura [1],Yuto Shimoirisa[2] , Shinichi Shioya[3]

ABSTRACT: We have been developing a frame system consisting of steel bar-timber composite members which can perform better than those of reinforced concrete structure. The steel bar is deformed bar, which is embedded near outer within the cross-section of the composite member and bonded with epoxy resin adhesive. Bending stiffness of the composite member is estimated to be approximately five times as much as conventional glulam timber for beam and approximately twice for column. Also, the bending strength capacity of the composite member is estimated to be approximately three times for beam and approximately twice for column. We, in the past, developed both wet and dry methods for connecting column and beam, and now we have been improving the latter method. The improvements include a new manufacturing process for the composite timber, a change to threaded steel bar, a change in the shape of the steel parts used for the connection, and a change to steel damper. This paper presents the improvements, those advantages, and a loading test to investigate the performance of the improved connection.

KEYWORDS: Glulam timber, Composite member, beam, moment frame, column-beam connection

1 – INTRODUCTION

Nowadays, cross laminated timber (CLT) has been used for buildings. However, CLT often restricts planning of buildings because it is flat plate member. In order to improve the flexibility of the planning, higher stiffness and strength are desired for column and beam. We have been developing a frame system of steel bar-timber composite members which can perform better than those of reinforced concrete structure[1] and have been developing a method for the connection between columns and beams by using steel structure connection[2]. In the previous our method, both ends of rebar were machined thread; the threaded part was fixed to the steel part for the joint with nuts; friction dampers were incorporated in the lower flange of its H-shaped steel to dissipate energy during earthquakes. In this study, four modifications were attempted, and then a loading test was conducted to verify mechanical performances of the column-beam connection.

i) Up to now, the composite beam has been manufactured by embedding and gluing rebars into laminas and then gluing the component lamina together. The workload in gluing the rebars was heavy and the loss of adhesive for the rebar was significant. To alleviate this problem, we improved the method for manufacturing glulam timber such as it has holes into which rebars can be inserted. This allows more accurate positioning of the rebars, so that it is easier to insert the rebars at the end of the beam into holes of the steel joint part. These details of mufacturing the timber are refer to Refference[3].

ii) In order to simplify the joint between the rebar and the steel joint part, the beam was modified to use threaded rebar with spiral-shaped rib. The ends of the rebar can be inserted directly into holes of the steel joint part and secured to the part with specified nuts for the rebar (hereinafter referred to as "lock nut"), eliminating the need for threading of the ends of normal rebars. This increases the rigidity and capacity of the column-beam connection.

iii) On the other hand, the joint between the steel joint part and columns must also have sufficient joint capacity. However, the shear strength of wood in the column-beam joint panel is extremely insufficient in the conventional column-beam assemblage. We have devised a method for reducing the shear stress of the column-beam joint panel by modifying shape of the steel part used. Moreover, the shape will reduce the anchorage force of anchor bolt from the steel joint part to the columns and increases the area for vertical shear force transmission at interface of column and the steel joint part.

iv) At beam ends in rigid-frame, moments due to long-term loading are large, and there are unresolved issues regarding the performance of friction dampers that receive such loads, especially creep characteristics after slippage, which will take time for practical application. This study employed a method of incorporating a steel damper, which is expected to fast become practical.

[1] Masanori Nakamura, Department of Architecture, Kagoshima University, Japan, k8869184@kadai.jp

[2] Yuto Shimoirisa, Department of Architecture, Kagoshima University, Japan, k3080536@kadai.jp

[3] Shinichi Shioya, Department of Architecture, Kagoshima University, Japan, k7347039@kadai.jp

https://doi.org/10.52202/080513-0455

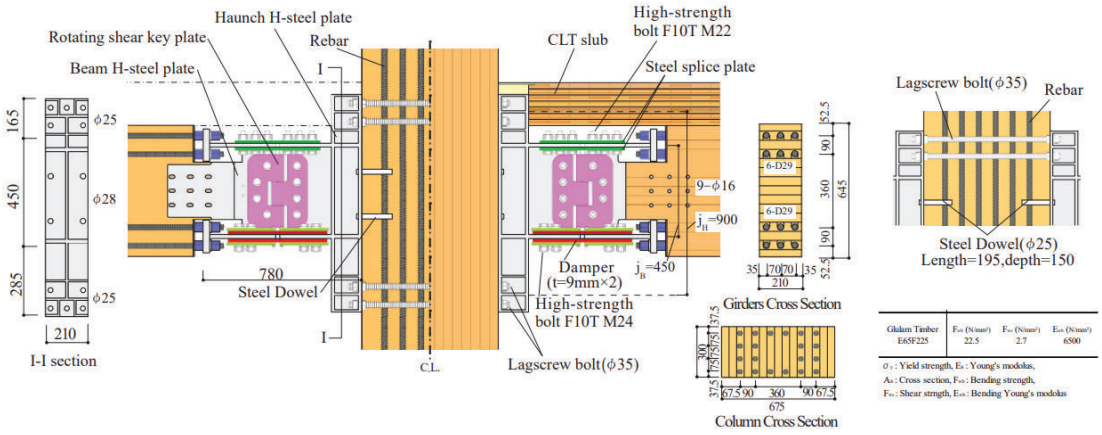

Figure 1 The connection of column and beam.

Although low-cycle fatigue failure is a concern for deformation history-dependent steel dampers, it is assumed here that they yield only during major earthquakes. Damage at the column-beam connection is assumed to be limited to the yielding of that steel damper only, and the deformation history of the damper is checked after the earthquake, and if low-cycle fatigue failure is a concern for the next large earthquake, the steel damper is assumed to be replaced.

2 – COLUMN-BEAM CONNECTION

Figure 1 shows the connection between column and beam. The column and beam are made of the composite member, and the steel joint part consists of two parts. One steel joint part connected to the column is haunch H-shaped steel part (hereinafter referred to as "haunch H-steel part") and the other part on the beam side is H-shaped steel part with two end plates welded to its upper and lower flanges and only its web plate is inserted into a slit gloved in the composite timber beam (hereinafter referred to as "beam H-steel part"). In the joint between haunch H-steel part and beam H-steel part, the upper flanges are connected with high-strength bolt friction joint using conventional splice plates; the lower flanges are connected with the friction joint using steel damper plates. The webs are connected with two pairs of shear key plates(rotational shear plate) that can transfer shear force while rotating. The center of the rotation is assumed to be at the center of clearance between haunch H-steel part and beam H-steel part and at the center height of the thickness of the upper flanges.

We are now considering two types of dampers: friction damper and steel damper, but in this study, only steel damper was selected. In the joint between column and haunch H-steel part, bending moment and axial force are assumed to be transferred by large-diameter lag screw bolts embedded in the column and its nuts, while vertical shear force is assumed to be transferred by dowel joint made of round steels. In beam H-steel part, bending moment and axial force are transferred to the end plates of the upper and lower flanges with threaded rebars and its nuts, while shear force is transferred by drift pins driven over the web steel plate that are inserted into the slit gloved in the beam's web timber.

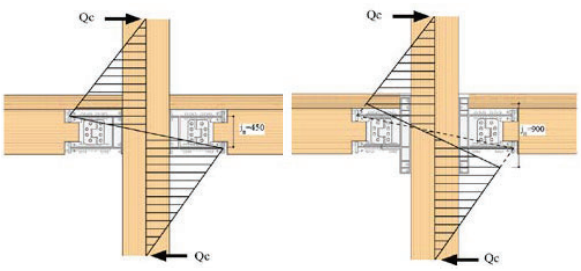

(a) Previous connection *(b) Proposed connection with haunch H-steel part*

Figure 2 Schematic diagram of bending moment distribution of columns.

3 – EFFECTIVENESS OF HAUNCH H-STEEL PART

3.1 REDUCATION OF SHEAR STRESS IN COLUMN-BEAM JOINT PANEL

Figure 2 shows schematically the distribution of the bending moment of column around a column-beam joint in a rigid frame subjected to horizontal forces. The case is illustrated with a story height h of 3.5 m and a beam height D_B of 625 mm and a internal lever arm j_B of 450 mm in beam. The beam section can support vertical load for a long span of 10 m with width of 4 m in design. Figure 2(a) shows a case without haunch H-steel part. Because the gradient of the bending moment can be regarded as the shear force of the column, direction of the shear force in the range of the column-beam panel is opposite to that in the column above and below, and the magnitude multiplier is {(h-jB)/2}/(jB/2), which is 6.78 times for the dimension mentioned above. Even if the joint strength capacity of the column and beam can be increased, shear failure will occur in the panel of the column-beam connection, and the bending capacity of the composite beam cannot perform efficiently in earthquakes. In this study, as shown in Figure 2(b), the j_H is increased by a factor of 2.0 for the haunch H-steel part, and the shear force ratio of the panel to that of the upper and lower columns can be reduced to 1/2.8.

3.2 REDUCTION OF AXIAL FORCE OF LAG

https://doi.org/10.52202/080513-0455

SCREW BOLTS IN COLUMN

When j_H is increased by a factor of 2.0 using haunch H-steel part, the pull-out and push-in forces of lag screw bolt (LSB) in the column caused by the bending moment transmitted to the columns at the haunch H-steel part can be also reduced by a factor of 1/2.0, thereby reducing the number of LSBs.

3.3 BOOST OF JOINT SURFACE AREA BETWEEN COLUMN AND HAUNCH H-STEEL PART

The boost of increased joint area between column and haunch H-steel part increases the vertical shear capacity of the joint of the column and beam because larger dowels can be used in the flange on column side of the haunch H-steel part. This makes it possible to readily transmit the shear force of long-span beam to the columns under long-term loading.

3.4 EFFECTIVENESS OF THREADED REBAR

By using threaded rebar for beam, the end of the rebar can be rigidly secured to the end plate of the beam H-beam flange with rock nut. Because there is no need to cut screws on the end of rebar, there is no loss of cross-section of rebar and the siffness and joint capacity of the rebar can be maximized. In this joint, the axial strength capacity of the damper is assumed to be approximately 60% of yield capacity of the lower rebars to avoid yielding of the rebars. The higher stress of the rebar leads to an increase in capacity expectable to the damper.

4 – LOADING TEST OF BEAM CONNECTED TO REACTION FRAME

4.1 SPECIMEN

Figure 3 shows cross section and side of the specimen. Figure 4 shows arrangement of rebars in the glulam timber. The specimen was selected to be full-scale. One specimen was tested. The material and thickness of the steel damper were planned as variables. In this chapter, the experimental results of one type of damper are presented. Glulam timber was E65F225 in Japanese Agricultural Standard, Japanese cedar/symmetrical cross-section of different grades. Resorcinol adhesive was used for gluing laminas. The threaded rebar was SD390 of D29(diameter) and the steel damper was LYP-225 of low-strength yield steel plate.

Figure 5 shows the shape and dimension of the damper. The damper was formed by laser cutting. To avoid larger errors in laser cutting when the thickness of steel plate is greater than 16 mm, a 9-mm-thick steel plate was cut and stacked in two pieces to make an 18-mm-thick damper. It was selected that the axial capacity of the damper at tensile rupture would be approximately 37% of the yield capacity of the lower end rebars. This was assumed so that shear stress at the column-beam joint panel can be less than the shear strength of timber.

Table 1 shows mechanical properties of rebar and damper steel by tensile tests. The sum of yield strength capacity of the six rebars is 1698kN, the yield capacity of the damper for the gross cross-sectional area of the yield section is 419.1kN and the tensile rupture capacity is 625.7kN. Shear strength capacity transmitted by the drift pins is 277kN in

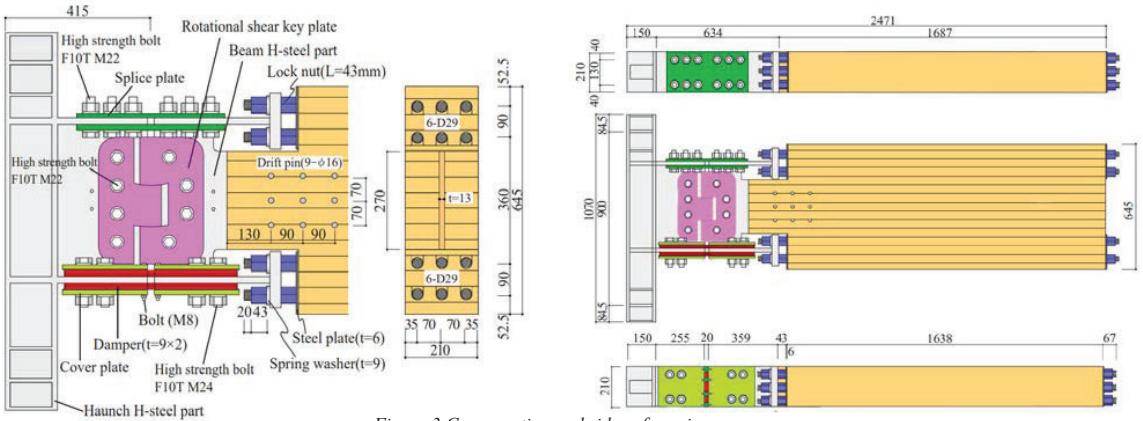

Figure 3 Cross section and sides of specimen.

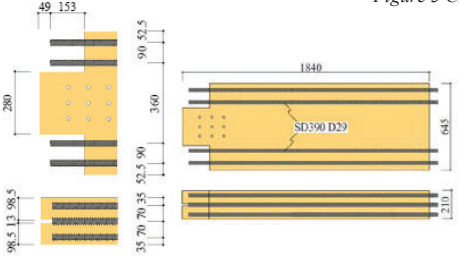

Figure 4 Arrangement of rebars in timber.

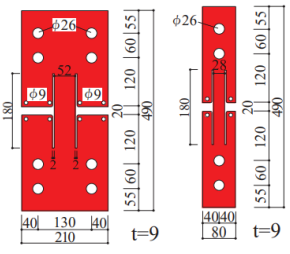

(a)DamperA (b)DamperB

Figure 5 Steel damper.

Table 1 mechanical properties of rebar and damper steel by tensile

Rebar D29-SD390	Es 1.90×10^5	σy 441.1	σu 629.4
Damper steel LYP-225	Es 1.48×10^5	σy 215.6	σu 321.9

Es:Young's modulus
σy:Yeild strength
σu:Tensile strength

https://doi.org/10.52202/080513-0455

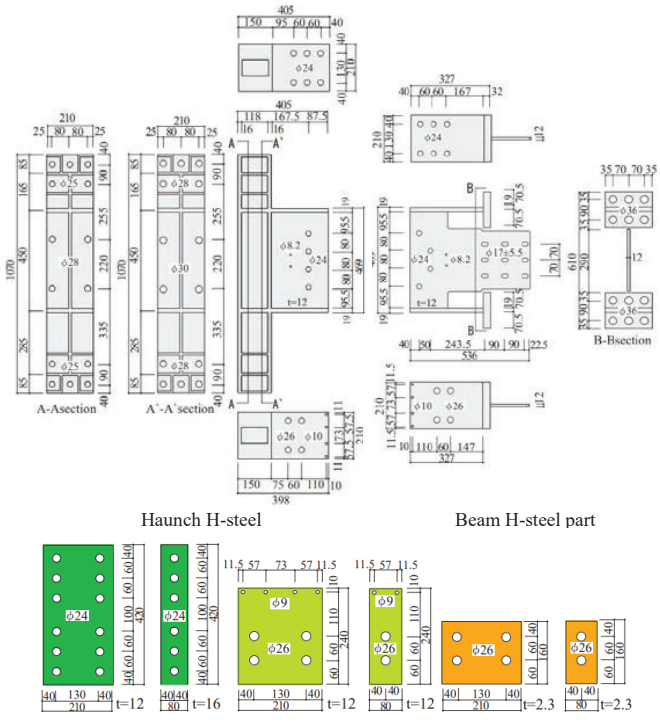

Figure 6 Parts for column and beam connection.

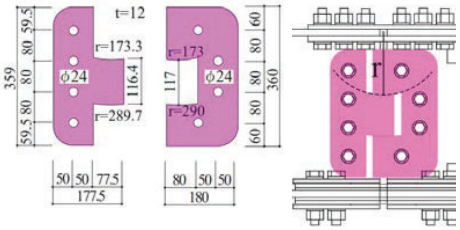

Figure 7 The shapes and dimensions of a pair of rotational shear plates.

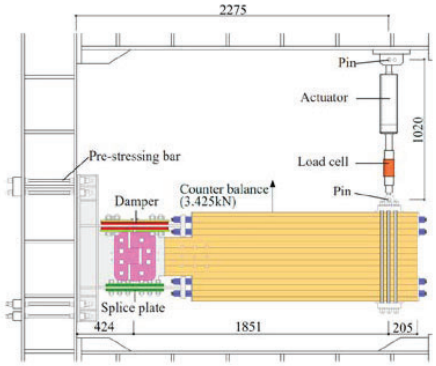

Figure 8 Set up for loading.

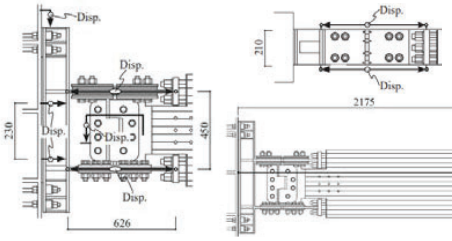

Figure 9 Positions for displacement transducer.

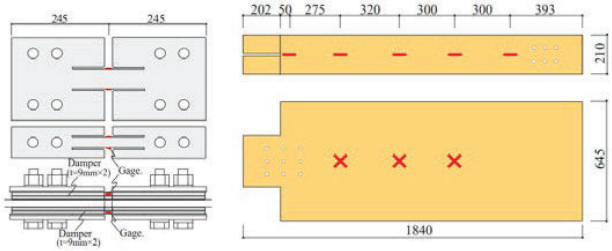

Figure 10 Positions for foil strain gauge.

total. The drift pins were made of S45C hardened and treated by heating, those having a diameter of 16 mm and a length of 210 mm.

Figure 6 shows the shapes and dimensions of haunch H-steel part, beam H-steel part, and components for the connection of column and beam. The flange and web were assembled and welded to form a single H-shaped steel, which was then cut to produce haunch H-steel part and beam H-steel part. Cutting of the web plate and machining of long holes for the drift pins in web plate of the beam H-steel were also formed by laser cutting. The width of the long hole was selected to be 17 mm against the drift pin diameter of 16 mm. The length of the long holes was selected to allow the drift pins to move up to ±5 mm in the axial direction of the composite beam. This reduces the bending moment transmitted by the nine drift pins to zero and to allow the drift pins to resist only shear force of the beam.

Figure 7 shows the shape and dimension of a pair of rotational shear key plates that transmits shear force between webs of haunch H-steel part and beam H-steel part. The pair of rotational shear key plates was joined with high-strength bolt friction joint to both the front and back surfaces of the webs.

The rotational shear plates were also made by laser cutting. The convex and concave blades are formed to fit each other. The clearance between both the blades was selected to be 0.6 mm in the normal direction from the center of its rotation. The material of H-steel part was SM490, and the other steel plates were SS400. All friction surfaces of the friction joint were sandblasted.

4.2 LOADING AND MEASUREMENT

Figure 8 shows set up for loading. Owing to the limited dimensions of the reaction frame, the beam was fixed to the reaction frame with their top and bottom sides inverted. In other words, the flange for the steel damper side was arranged to be upper and the flange for the splice plate side was done to be lower. The haunch H-steel part was also inverted up and down accordingly. The haunch H-steel part was joined to the reaction frame by four high-strength bolts at the upper and lower positions to resist the bending moment of the beam and to transmit vertical shear force, but in this experiment, steel plates fixed with high-strength bolts

https://doi.org/10.52202/080513-0455

were placed on the top and bottom faces of the haunch H-steel part to prevent its vertical slippage. Cyclic-reversed vertical loading was applied to the right-side end of beam.
A vertical uplift force was applied at the center of gravity of weights of the composite beam part and the beam H-steel part, in order to counteract the moment at position of the center of damper by the weight of beam. Figure 10 shows set up of measurement of strains: axial strain (gauge length:60mm) at flange surface of timber, shear strain at web of timber, and axial strain at the yielding section of the damper.
Figure 11 shows protocol of target deformation angle Rt for each cycle. The first and the second cycles were load-controlled with targets of ±30kN and ±60kN, respectively, and thereafter the target deformation angle Rt was set and the force was applied cyclically with a gradual increase.

5 – EXPERIMENTAL RESULTS

5.1 RETIGHTENING OF NUTS ON HIGH-STRENGTH BOLTS OF THE DAMPER AND INSTALLATION OF STEEL PLATES PREVENTING BUCKLING OF THE DAMPER

As seen in Figure 3, both ends of the damper are friction-jointed with the flange by high-strength bolts. It was observed that buckling occurred at the yield section of the damper and the protrusion of its buckling caused out-of-plane deformation of the cover plate. At this stage, the nuts of the high-strength bolts were loosened and a 2.3 mm plate (buckling-preventing plate) was inserted into the 2.3 mm gap between the damper and the cover plate as shown in Figure 12, and the nuts of the high-strength bolts were retightened. The 2.3 mm gap is designed to prevent the increase in the compressive capacity of the damper during compression-yield without restraining the increase in damper thickness caused when the yield section is compressed. The buckling-preventing plate is intended to prevent buckling by restraining the position where the buckling mode of the yield section protrudes the most, and to prevent an increase in the compressive capacity of damper by reducing the area where the increase in damper thickness is restrained. After having retightened the nuts of the high-strength bolts, the same deformation angle was used to apply reversed cyclic loading three times. After this, no slip of the friction joints of damper and no buckling of the yield section occurred.

5.2 SHEAR FORCE -DEFORMATION ANGLE RELATIONSHIP OF BEAM

Figure13 shows shear force-deformation angle relationship as beam. The deformation angle is the vertical deformation of the beam (in Figure 9 right) divided by the horizontal distance (2175 mm) from the force-applied point to the column of the reaction frame to which the beam is joined. Figure 13(a) shows all loops from the beginning of loading to final failure. Loops from the beginning of the damper's friction-joint sliding noise to the retightening of the high-strength bolt nuts are shown in orange, and loops after those are shown in blue. Various loops indicated below are also shown in same colors.
The damper is in compression on the positive loading and in tension on the negative loading. The shear forces computed from the bending moment based on strengths of tensile yield and tensile rupture of the damper steel shown in Table 1 is indicated by pink and red dashed lines, respectively. The shear forces at yielding, in both positive and negative loading, are in close agreement with the calculated shear forces. The maximum shear force is in close agreement with its calculated value on the negative. However, the increase in capacity after yielding on the positive is larger than that on the negative and the maximum force on the positive exceeds its value red dashed line. It might have been possible that the buckling-preventing plate restricted the increase in thickness of the yield section of the damper. Further investigation is needed to determine appropriate shape and dimension of the buckling-preventing plate. Future studies should also include the compressive strength of the damper steel, and the strain history of the yield section of the damper.
After application of the cyclic loading up to $2.0x10^{-2}$ rad. was completed, one-way loading was conducted in the direction of the negative loading where the damper was in tension. The maximum capacity was reached at $2.24x10^{-2}$rad. and the damper began to sound like a rupture noise at $2.57x10^{-2}$rad. The strength capacity after this decreased simultaneously with the several rupture noises. Although it is not possible to conclude because of the slip of the damper joint, the damper probably be able to exhibit its performance without rupturing under a large earthquake up to $\pm 2.0x10^{-2}$ rad..
Figure 13(b)-13(f) show representative loops. As shown in Figure 13(c), the damper yielded at 0.75x10-2rad. When re-loading in the opposite direction from the unloading, the phenomenon of slip on the loops, in which the deformation returned to zero with a small force, occurred.
Figure 14 shows the moment-rotation angle relationship between haunch H-steel part and beam H-steel part joint. The moment is the value at the center of the clearance

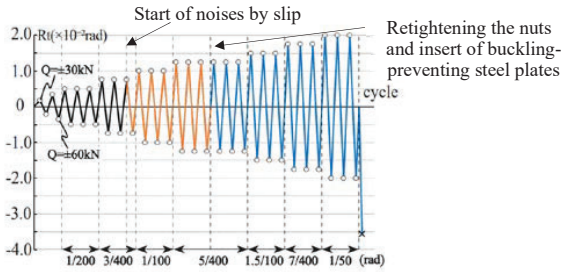

Figure 11 Protocol for displacement of beam.

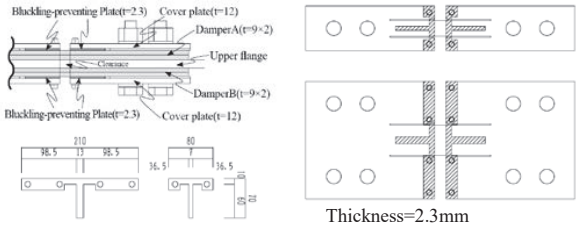

Figure 12 Buckling-preventing steel plates(Unit:mm)

https://doi.org/10.52202/080513-0455

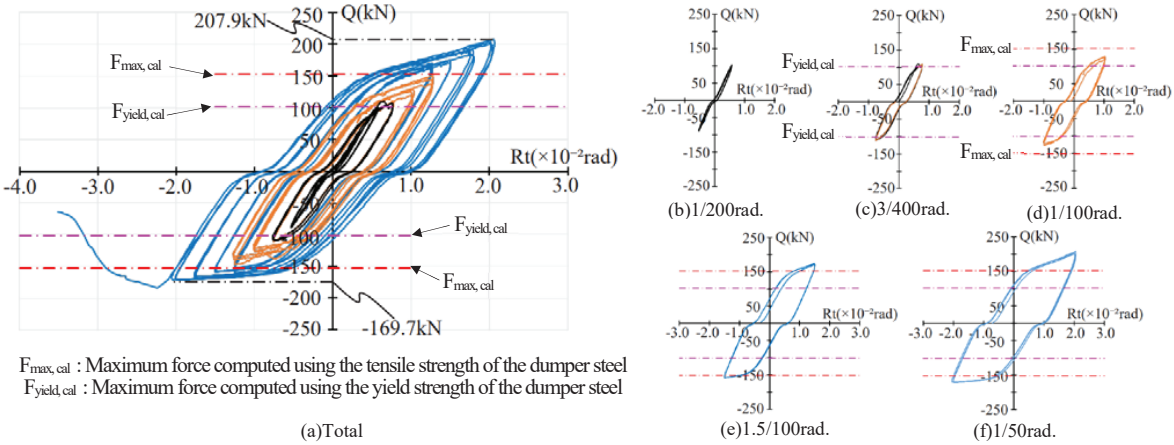

$F_{max,cal}$: Maximum force computed using the tensile strength of the dumper steel
$F_{yield,cal}$: Maximum force computed using the yield strength of the dumper steel

Figure 13 Vertical force-deformation angle relationship.

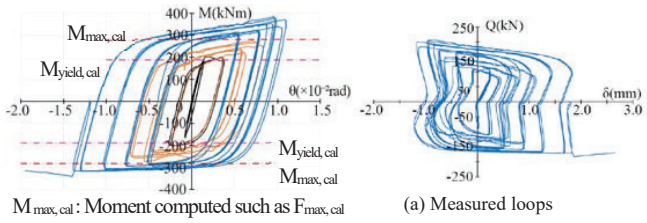

$M_{max,cal}$: Moment computed such as $F_{max,cal}$

Figure 14 Moment-rotation angle loop of joint of haunch and beam H-steel parts.

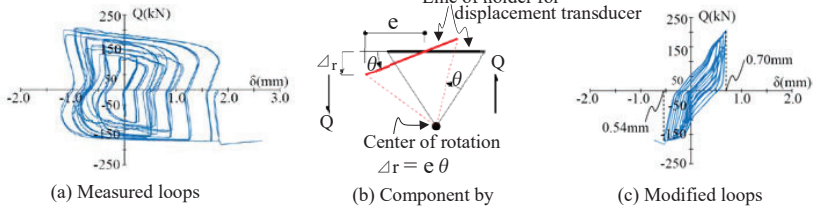

Figure 15 Shear force-vertical deformation relationship of Haunch H-steel part and beam H-steel part.

between the two H-steel parts. The rotation angle is computed from the axial deformation of the flange in Figure 9. The loops indicate elastoplastic with the yield moment increasing with the cyclic loading in Figure 11.

Figure 15(a) shows the vertical deformation between the haunch H-steel part and beam H-steel part webs by displacement transducer against the beam shear force. The deformation is the average δ_{vo} of those of the front and back displacement transducer. This amount of δ_{vo} includes a component of rotation with the center of rotation being the lower flange when the damper yields in compression or tension. To extract the vertical deformation, it is necessary to remove the rotational component.

Figure 15(b) shows the vertical component of the deformation/Δ_r due to rotation of angleθ. The change in deformation after subtracting Δ_r from δ_{vo} is shown in Figure 15(c) The peaks of loops of the 2.0×10^{-2} rad. are approximately -0.54mm or +0.7 mm. Although bias occurs, those are an extremely small deformation. The clearance between the blades of a pair of the rotational shear key plates is designed to be 0.6 mm, and without bias, a slip of ±0.3 mm at least would occur. If the blade is assumed to be a cantilever and the shear force of the beam is assumed to be 200 kN, the computed elastic deformation is about 0.1 mm, where the length of the cantilever is assumed to be 60 mm. The sum of these values is expected to be ±0.4 mm. If this values are added to the clearance slip of ±0.3 mm mentioned above, we get ±0.7 mm, which is almost the same as the experimental value of -0.54 mm or +0.7 mm.

Figure 16 shows axial strain distributions at the upper and lower surface of the timber. A vertical dashed line is shown at the location with the same dimension as the beam depth, on the left-hand side from the edge of the timber in the horizontal range. This location has been reported as the boundary where the rebar and glulam timber are fully integrated to resist, with the plane section under bending being valid. In the range from the position to the force-applied point, the strain distribution varies almost linearly.

Figure 17 shows moment-curvature relationship at each position of the strain gauges. The curvature was calculated from the foil strain gauge values. The bending stiffness relationship calculated using specified values of Young's modulus for the rebar and glulam timber is shown by an orange dashed line. At the three locations on the right-hand near the force-applied point, the line of the calculated stiffness is in close agreement with experimental stiffnesses.

Figure 18 shows shear stress-shear strain relationships. The shear stress was assumed to be the value at the middle height of the beam height, taking into account the rebar, and its shape factor for shear stress was assumed to be 1.45. The shear strain was obtained from the cross gauge. The slopes of the shear modulus at the beginning of the experiment are shown by the dashed lines. The values/Gw of the slope are 1.48-1.70 times as many as the specified value of shear modulus of elasticity, i.e., 433 N/mm^2.

Figure 19 shows the relationship between the moment and angle of rotation of the node of haunch H-steel part. The angle of rotation was obtained from the deformation of the two displacement transducers at the joints shown in Figure 9 left-hand. The moment-rotation angle relationship based on the elastic theory is also shown in the Figure 19, by an orange dashed line. The stiffnesses in positive and negative unloading are in close agreement with the calculated stiffness. The upper and lower parts of haunch

https://doi.org/10.52202/080513-0455

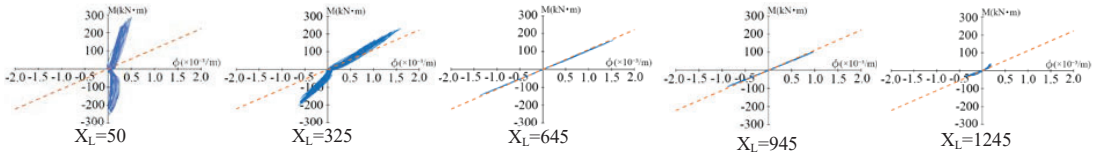

Figure 17 Moment-curvature relationship of the composite beam by foil strain gage.

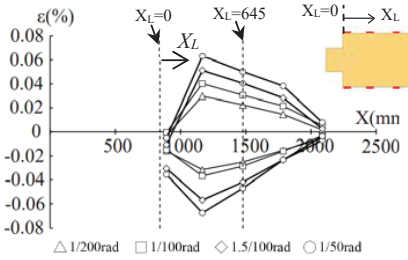

Figure 16 Distribution of axial strain on upper and lower surface of timber.

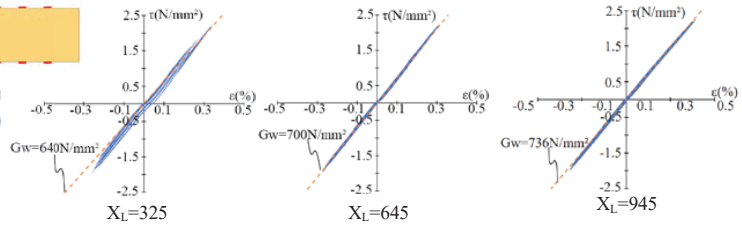

Figure 18 Shear stress-shear strain relationship of web of timber

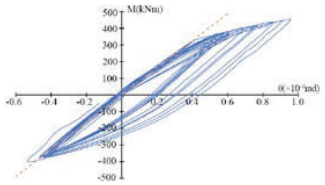

Figure 19 Moment-rotation angle loop in the haunch H-steel part

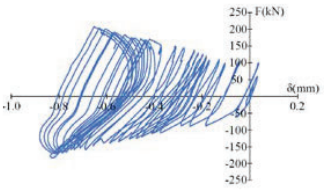

Figure 20 Shear force -vertical slip deformation relationship at top of haunch H-steel part.

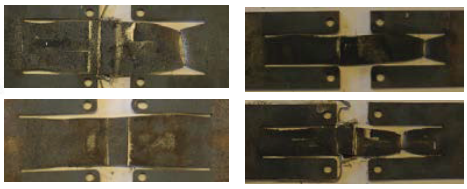

(a)DamperA (b)DamperB

Photo 1 Steel damper after loading test.

H-steel part were tightened with high-strength bolts to the reaction frame, between which a 9 mm thick steel plate was sandwiched each to allow deformation of Haunch H-steel part. In addition, the haunch H-steel part was set be in contact with anti-slip steel on the upper and lower surfaces. Friction is considered to occur on the contacting surfaces due to the cyclic loading, causing hysteresis loops. At the positive maximum force, the angle of rotation of the node was 0.95×10^{-2} rad. This indicates that the rotation of the node of the haunch H-steel part has a significant effect on the deformation of the beam. This was led to the delay of the yield deformation of the damper up to 0.75×10^{-2} rad. and the increase of the deformation at the damper's rupture up to 2.57×10^{-2}rad. This suggests that the yield deformation and the rupture deformation of the damper of the composite beam can be adjusted by the thickness of the flange of haunch H-part.

Figure 20 shows the relationship of shear force and vertical slip deformation between the haunch H-part and the column of the reaction frame. The slip was obtained from deformation by displacement transducer at the top of haunch H-steel part as shown in Figure 9. The haunch H-steel part moved upward by about 0.8 mm due to the cyclic loading. There may have been a small gap between the bottom surface of the haunch H-steel part and the contact surface of the anti-slip steel. In the actual structure, the vertical slip will be stopped by dowels made of round steel. This suggests that the slip must be included in the deformation of the composite beam.

Photo 1 shows the damper taken out of the specimen after test was completed. Damper A was observed to have raptured in one of two pieces, and damper B was observed to have ruptured in all the four pieces. All ruptured positions were at one end of the yield section rather than at the axial middle of the section. There were also areas of swelling in the width direction due to compressive yielding. However, there was no situation where its swelling was restricted by the steel plates on both sides. It can be concluded that a slit width of 2 mm on both sides of the yielding section of damper A is sufficient. Damper B was observed to might have buckled in the in-plane direction. As the width of the yield section is only 28 mm against swelling in the width direction, it is considered that the width of the slits on both sides should be smaller than 2 mm, preventing the progression of buckling deformation.

6–ADDITIONAL LOADING EXPERIMENTS

We conducted additional two experiments to investigate for mild steel damper of grade=SS400,hereafter, the second loading experiment. Moreover, both ends of the yield section of damper was improved to be on a circular arc to alleviate stress concentration at the end of the yield section,hereafter, the third loading experiment. All parts of the specimen used in the first test were used except for the dampers.

6.1 IMPROVEMENT OF DAMPER

Figure 21 shows the shape and dimension of the dampers. Table 2 shows the mechanical properties of damper as determined by tensile testing. The loading protocol to the specimen is shown in Figure 22. The loading was conducted as well as Section 4.2. Photo 2 shows the damper ruptures. Cracks were observed at the ends of the

https://doi.org/10.52202/080513-0455

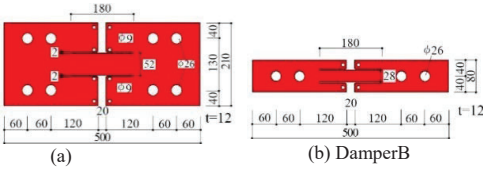

Figure 21 Steel damper for 2nd experiment(Unit:mm)

Table 2 Mechanical properties of rebar and steel damper for 2nd experiment by tensile

	Fs(N/mm²)	σy(N/mm²)	σu(N/mm²)
Rebar D29-SD390	1.90×10⁵	441.1	629.4
Steel damper (2nd experiment)	1.80×10⁵	290	464

Es:Young's modulus
σy:Yeild strength
σu:Tensile strength

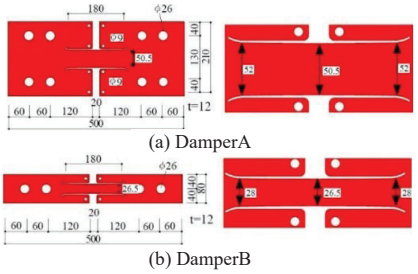

Figure 23 Steel damper for 2nd experiment(Unit:mm)

Table 3 Mechanical properties of rebar and steel damper for 3rd experiment by tensile

	Es(N/mm²)	σy(N/mm²)	σu(N/mm²)
Damper steel (3rd experiment)	1.93×10⁵	280.5	462.0

Es:Young's modulus
σy:Yeild strength
σu:Tensile strength

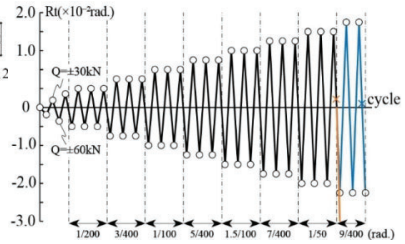

Figure 22 Protocol for displacement of beam

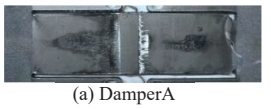

(a) DamperA

(b) DamperB1

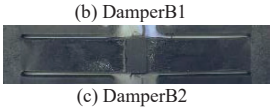

(c) DamperB2

Photo 2 Steel damper after 2nd experiment

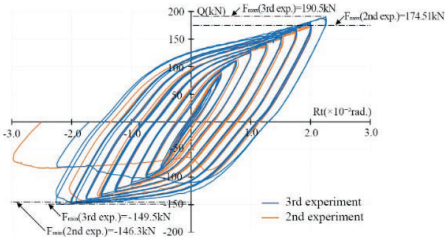

Figure 24 Vertical force-deformation angle relationship

(a) DamperA

(b) DamperB1

(c) DamperB2

Photo 3 Steel damper after 3rd experiment

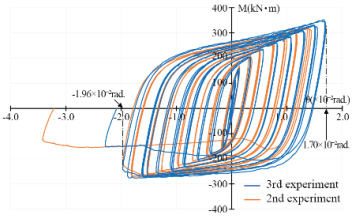

Figure 25 Moment-rotation angle loop of joint of haunch and beam H-steel parts

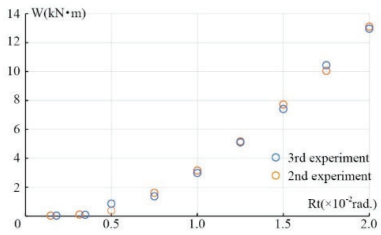

Figure 26 Dissipation energy-deformation angle relationship

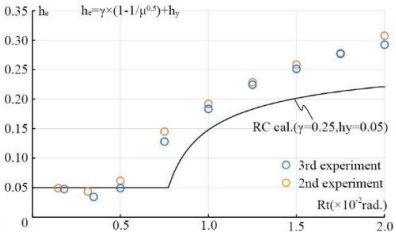

Figure 27 Equivalent viscous damping ratio he-deformation angle relationship

yield section of all dampers. This was probably due to the stress concentrating at the end of the damper before the damper reached its tensile rupture capacity, causing the crack to form. As in the first loading test, the center of the yielding section swelled in the width direction. From these results, in order to alleviate stress concentration and increase in strength on the compression side due to swelling, the third force experiment was conducted using a damper with a modified shape of the yield section.

Figure 23 shows the shape and dimensions of the damper. The steel grade was SS400 with a thickness of 12 mm. In order to prevent stress from concentrating at the ends, the shape was made like an arc, like a material test specimen. In the first loading experiment, it was confirmed that the center of the yield section of the damper swelled in the width direction. Therefore, the width of the yielding section was made to become narrower at the center of the yielding section. The width of the center section was made 1.5 mm thinner than in Figure 21.

Table 3 shows the mechanical properties of the damper as determined by tensile testing. The specified yield strength capacity of the damper for its total cross-sectional area is 348 kN, and the specified tensile rupture capacity is 573 kN. Photo 3 shows failures. The cracks at the ends of the yielding section were prevented, but the yielding section was not prevented from bulging.

6.2 FORCE-DISPLACEMENT RELATIONSHIP

Figure 24 shows shear force-deformation angle relationship. The curve of the second experiment is shown in orange, and one of the third experiment is shown in blue. In the second experiment, after cycle at 2.0×10^{-2}rad. was completed, loading was applied in the negative force direction. On the other hand, in the third experiment, the damper ruptured and the load capacity decreased at -2.25×10^{-2}rad. The deformation angle at which the damper ruptured increased in the third experiment compared to the second experiment. This result demonstrates the fact that the rupture due to stress concentration at the edge of the yield section was prevented. In the second experiment, the shear force-deformation angle relationship of the first test did not show the phenomenon of slipping at a light load when the damper was reloaded in the opposite direction

https://doi.org/10.52202/080513-0455

from the reduced force. This can be attributed to the use of ultra-high-strength high-strength bolts for the friction joints between the damper and plate, which increased the frictional force and prevented the damper plate from slipping. Also, the locknuts did not loosen.

Figure 25 shows the moment-rotation angle relationship. The color correspondence of the curves are the same as in Figure 24. In the third experiment, the rotational angle of rotation is only 1.70×10^{-2} rad. for the positive force side, while it is 1.96×10^{-2} rad. for the negative force side. This is due to the difference in the rotational stiffness of the joint under positive and negative forces.

Figure 26 shows the dissipation energy-deformation angle relationship, and Figure 27 shows change of equivalent viscous damping ratio h_e for each target deformation angle. There was no difference in energy consumption performance between the second and third experiments, and no difference was caused by differences in damper geometry. The equation for h_e used in the design is shown in the Figure 27. For reinforced concrete (RC) beams, γ = 0.25, and the resulting curve is shown by the solid black line. Compared to conventional RC beams, it is higher.

6.3 BEHAVIOUR OF DAMPER

Figure 28 and Figure 29 (a)-(c) show the relationship between the shear force and axial strain of each plate of the damper. The strains are the average of the values of two foil gauges (length: 2 mm) in the yield section shown in Figure 10. The calculated yield loading is shown in the figure as a horizontal pink dashed line, and the load at tensile rupture is shown as a horizontal red dashed line. The strength of steel used in the calculations was based on material test value. The calculated shear of the beam at yield and fracture is close to the experimental results.

In Figure 28(a),(b),(c) and Figure 29(b), the center of the loop is skewed toward the compression side. Figure 28 and Figure 29 (d) show the relationship between the axial deformation of the damper side flange and the shear force of the beam. The axial deformation is the average of the two displacement transducer values of the damper side flange as shown in Figure 9. In this relationship there is no bias toward the center of the loop. The absolute value of the compressive deformation is small relative to the value of the negative force, even though the positive force load is larger than the negative force in the final loop. The secondary stiffness of the steel damper after yielding suggests that compression is higher relative to tension.

The deformation of the peak of the loop just before rupture was 8.68 mm in the second force experiment and 8.59 mm in the third force experiment. When these are divided by the 180mm of the yielding section, the strain becomes 4.82% and 4.77%. At this strain, the specimen did not fracture until three repetitive stresses were applied. Takeuchi[4] et al. also reported that ordinary steel dampers rupture after 5 repetitions of ±5%. The results of this experiment were similar to the results of Takeuchi .

6.4 BEHAIVUOR OF ROTATIONA SHEAR KEY

The center of rotation of the rotational shear key plate in

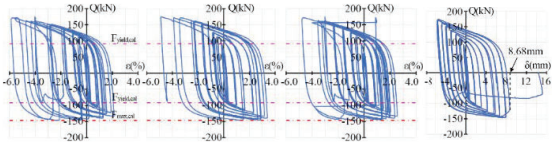

(a) Damper A (b) Damper B1 (c) Damper B2 (d) Flange fo damper

Figure 28 Shear force-damper strain selationship for 2nd experiment

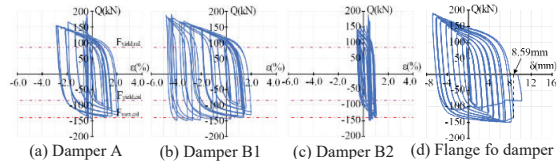

(a) Damper A (b) Damper B1 (c) Damper B2 (d) Flange fo damper

Figure 29 Shear force-damper strain selationship for 3rd experiment

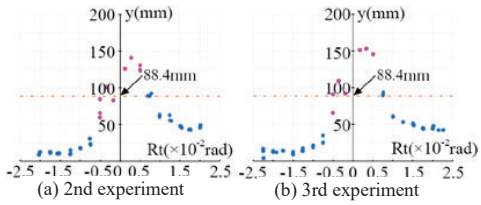

(a) 2nd experiment (b) 3rd experiment

Figure 30 Rotation center position-target deformation angle relationship

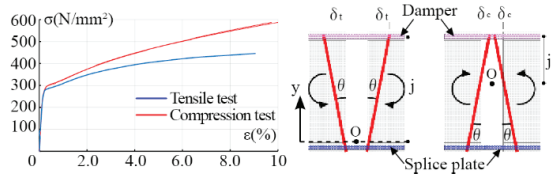

(a) Stress-strain curve (b)Formation according to rotation

Figure 31 Rotation center position-target deformation angle relationship

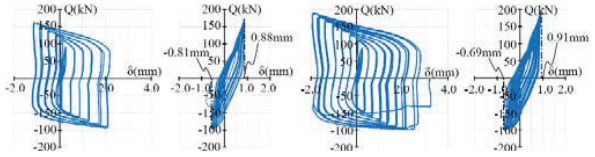

(a) 2nd experiment (b) 3rd experiment

Figure 32 Shear force-vertical deformation relationship of haunch H-shaped steel part and beam H-shaped steel part

Figure 7 was set at the center of the thickness of the flange on the splice plate side and at the center of the clearance between the Hunch H-beam and the beam H-beam. However, strictly, the center of rotation varies depending on whether the damper is resisting elastically or under yielding and resisting in tension, or in compression. The clearance between the two H-shaped steel beams absorbs the plastic deformation of the damper and its rotation. The center of rotation can be calculated using the value of the axial deformation of the upper and lower flanges: it can be assumed to be the height position at which the value of the line of the deformation is zero. Figure 30 shows the calculated height of the center of rotation at the peak of each cycle. The horizontal axis is the target deformation angle Rt. On the positive side, the damper resists compression and on the negative side it resists tension.

The neutral axis from the calculation for the case where the splice plates and steel dampers of the upper and lower

https://doi.org/10.52202/080513-0455

flanges resist elastically is shown by the horizontal orange dotted line. Symbol ● indicates that the force did not exceed the yielding force of calculation shown in Figure 28 and Figure 29; symbol ● indicates for exceeding. The ● during elastic resistance is closer to the damper side flange. For in tenision, ● approaches the side of the flange that does not yield, and for in compression, ● approaches the center of the beam height. After yielding in bending, the shear force in the direction of the force that causes the damper to yield in compression becomes larger, and the shear force and bending moment of the rotating shear key plate also increase, so from the respect of minimizing the maximun moment of beam when the damper be in compresin, it is desirable to process the center of rotation of the rotating shear plate to match the center of rotation of the side that yields in compression.

As described in Section 6.3, even when the same positive and negative deformation angles were applied to the beam, the damper's axial deformation loop was biased toward the tension side, as seen in Figure 28(d)and Figure 29(d). Figure 31(a) shows the stress-strain relationship of the damper's SS400 steel from the material test.

The stress-strain relationship is for the uniaxial tension and compression test of each test piece made of the same material. The Young's modulus and yield stress were almost the same in tension and compression, but the secondary rigidity after yielding was greater in compression, and the compressive strength capacity was also extremely large, so the rigidity differed depending on the direction of the applied force.

Even with the same deformation angle, the shear force is different, so the deformation of the part except the damper is different, and the rotation angle of the damper position on the side of the negative load side, where the yield load is small, is larger than that on the positive load side. Also, as shown in Figure 30, the rotation center O is closer to the flange on the negative force side, where the damper yields in tension, than on the positive force side, where it yields in compression. The clearance between the left and right steel parts opens or closes with its rotating, around point O. This deformation state is shown in Figure 31(b).Even if the value of θ is the same for positive and negative, the distance j from the center of rotation to the damper is greater for the side that yields in tension, so the damper elongates more than the side that yields in compression, and it remains in a state of elongation on the tension side. As can be seen in Figure 28(d) and Figure 29(d), the maximum deformation of the damper increases as the deformation angle increases, and the negative force side, where the damper elongates, increases.

Figure 32 shows the relative vertical deformation between the web of the H-shaped beam and the H-shaped beam of the haunch, measured by displacement transducer, in relation to the shear force of the beam. The vertical displacements were calculated as well as Figure 15. The peak of the cycle just before rupture was -0.81mm or +0.88mm in the second loading experiment, and -0.69mm or +0.91mm in the third loading experiment. These experimental values are close to the calculations(±0.7mm) mentioned in Section 5.2.

7 – CONCLUSION

In order to investigate the mechanical performance of beam specimen with the developed dry connection method for the steel bar -timber composite beam and column, loading tests were carried out on a full-scale specimen under the assumption of a major earthquake. A low yield point steel damper and two different forms of normal mild steel SS400 were used for the beam end connections. The results are as follows.

i) In the column-beam connection, the proposed haunch H-steel part decreases shear stress of the column-beam joint panel and axial force of the bolts anchoring from the beam to the column and increases the interface area of the column and the flange of the haunch H-steel part. The reduction in stress and axial force is expected to be 58%.

ii)When steel dampers with low-strength yield steel plate were used, the dampers did not rupture even the large number of repetitive loading cycles up to $2.0\text{x}10^{-2}$rad. assuming a large earthquake. The components in the deformation of the beam were also revealed. The damper yielded at $0.75\text{x}10^{-2}$rad. and exhibited abundant energy dissipation.

iii)As the yielding section of the damper was affected by bending strain due to buckling, the proposed buckling-prevention plate should be used to prevent buckling,but the appropriate dimension of the plate with little restraint on the increase in thickness during compression-yield should be investigated.

iv) The rotational shear key plates were able to transfer shear force while rotating. The deformation component in the shear force direction was clarified and its deformation was confirmed to be extremely small.

v) It was found that even if the steel grade of the damper was changed from low yield point steel to SS400 steel, the damper showed similar performance under the cyclic loading force for a large earthquake.

vi)When steel dampers are subjected to repeated compression and tension at the yield load level, they do not deform uniformly in the yield section, and a phenomenon occurs in which the strain in the center of the yield section is biased toward the compression side. On the other hand, the average strain in the yield section did not show this bias. The strain at the point of rupture of the damper was approximately 4.8% in the yield section, and there was no difference in between a damper made of low-strength yield steel and a normal mild steel damper.

8 – REFERENCES

[1] S.Shioya, et al.: An innovative hybrid timber structure in Japan: performance of column and beam, Wein, WCTE 2016.

[2] K. Nagano, et al.: Experiment of a new connection between column and beam producing high-energy dissipation and re-centering, Santiago, WCTE 2021.

[3] Y.Shimoirisa,et al:Steel bar-timber composite beam-column connection adopting steel damper, Milan,WCEE 2024

[4] T. Takeuchi, et al: Cumulative deformation capacity and damage evaluation for elasto-plastic dampers at beams,in Japanese, J. Struct. Constr. Eng., AIJ, No.600, pp.115-122, Feb., 2006

https://doi.org/10.52202/080513-0455